Kufa Journal of Engineering
Vol. 12, No. 1, January 2021, P.P. 95-110
Received 30 September 2020, accepted 6 November 2020

NUMERICAL STUDY OF NATURAL CONVECTIVE HEAT TRANSFER WITHIN M-SHAPED ROOFS

Ola Kamiyo[1]

[1] Department of Mechanical Engineering, University of Lagos, Lagos, Nigeria.

Email: okamiyo@unilag.edu.ng

HTTP://DX.DOI.ORG/10.30572/2018/KJE/120107

ABSTRACT

Natural convective heat transfer in M-shaped roofs has been investigated using CFD approach with the aim of determining the flowfield and thermal characteristics of the attic when heated through the ceiling for pitch angles 14^o, 20^o, 25^o and 35^o and Rayleigh number between 10^6 and 10^7. The results show that the 'M' shape of the roof has strong influence on the airflow pattern and heat transfer. For all the roof pitches, counterrotating cells with varying intensities and thermal plumes are obtained. The air velocity variation laterally across the attic forms a sequence that mimics the flowfield thus enabling the relative size of a cell and its intensity at a position in an attic of a particular pitch to be predicted. The size of the twin vortices at the central area is found to increase by 4% with the roof pitch. As the pitch increases, the thermal plumes get thicker while their number reduces and heat transfer rate decreases.

KEYWORDS: Natural convection, Heat transfer, M-shaped, Triangular roof, Pitch Angle

1. INTRODUCTION

Investigations on the problems of natural convection in enclosures is important due to their engineering applications in roof designs, air conditioning, solar systems, cooling of electronic circuits and heat exchangers among others. In particular, studies on heat and fluid flow mechanisms in rooftops have focused on the effects of enclosure shapes and boundary conditions. The works of Flack (1980) and Akinsete and Coleman (1982) on the experiment and simulation of pitched rooftop models, respectively, laid the foundation for more investigations on pitched roofs in form of triangular enclosures. Kamiyo *et al*. (2010), Saha (2011) and Das *et al.* (2017) presented broad reviews on regular pitched and some complex-shaped roofs that cover the effects of roof configurations which result in various flow regimes. Thereafter, investigations based on different approaches have continued. However, with the development of advanced numerical methods that could accurately predicted problems of flows in enclosed surfaces, majority of the authors have used modelling approach. In the past decade, the numerical modelling studies reported include those of Wang *et al.* (2012), Wang and Shen (2012), Ching *et al*. (2012), Yesiloz and Aydin (2013), Kamiyo *et al*. (2014), Mirabedin (2016) and Amrani *et al.* (2017) while the few experimental studies are those of Anderson *et al*. (2010), Oztop *et al.* (2012), Yesiloz and Aydin (2013), Raj *et al.* (2018) and Michels *et al.* (2018). In most cases, sealed attics are considered but there are few reports on vented attics (Wang *et al.* (2012), Wang and Shen (2012), Raj *et al.* (2018)).

In attempts to model different weather scenarios, a number of studies have considered different thermal boundary conditions. Enclosure heated from below only is reported by Asan and Namli (2001), Mahmoudi (2011), Kamiyo *et al.* (2014) and Cui *et al.* (2019). Enclosure heated from above only is studied by Akinsete and Coleman (1982), Asan and Namli (2000) and Amrani *et al*. (2017). Ridouane *et al*. (2005), Mahmoudi *et al.* (2013), and Yesiloz and Aydin (2013) considered both concurrently. Special boundary conditions are applied by Saha *et al*. (2010a) - periodic thermal forcing, Saha *et al.* (2010b) - instantaneous and ramp cooling, Saha and Gu (2015) - non-uniform cooling and Triveni *et al.* (2015) - partially heated walls.

Recently, some complex roofs reported include dome (Das and Morsi, 2002), inclined triangular cavity (Mahmoudi *et al*., 2013), asymmetric triangular cavity (Kamiyo *et al*., 2014) and baffled triangular enclosure (Saha and Gu, 2015). Others are vertical upright–angled triangular cavity (Sieres *et al*., 2016), gable roofs (Wang *et al*., 2012; Amrani *et al*., 2017), sectioned-triangular prismatic enclosure (Cui *et al*., 2019) and trapezoidal enclosure (Mehryan *et al*., 2020). Many other complex-shaped roofs have been studied but there are still some common ones that require further investigations. In this study, natural convective heat transfer in M-shaped roof heated from the horizontal bottom wall, as shown in Fig. 1, is investigated for pitch angles 14^o, 20^o, 25^o and 35^o within the range $1.14 \times 10^6 \le Ra \le 2.74 \times 10^7$. The objective is to apply a numerical technique to better understand the effect of the M-shaped roof on the airflow pattern and heat transfer within the attic bearing in mind engineering application benefits.

Fig. 1. M-shaped roof house

2. METHODOLOGY

The physical geometry of the M-shaped pitched roof investigated in this study, which coincides as the computational domain, is as shown in Fig. 2 in two-dimensional form. According to Penot and N'Dame (1992), the geometry of a pitched roof could adequately be represented by a two-dimensional triangular shape provided the roof extension in the direction perpendicular to the cross-section is more than double its width. The geometry forms the 'M' shape with the upper vertex of a standard triangle inverted at four-fifth of its height. Hence, for a unit length L, height H is two-fifth of the tangent of the pitch angle or of the aspect ratio. This complex shape of the roof is expected to influence the airflow pattern and thermal characteristics of the attic. The full geometry is considered in order to avoid problems associated with symmetry assumptions highlighted by Holtzman *et al* (2000). The enclosure is filled with air and there is no internal heat generation. The flow is steady and Bousinessq model applies. The validity of invoking the Bousinessq model is substantiated by Gray and Giorgini (1976) and Ridouane *et al*., (2005). The computational domain dimensions and boundary conditions are normalized as real life roof sizes and weather conditions vary.

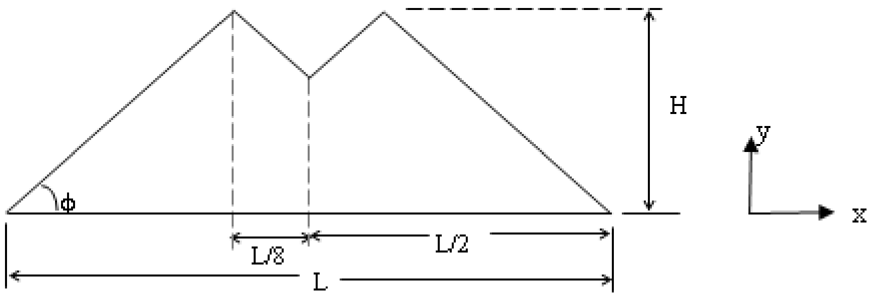

Fig. 2. Physical model.

The dimensionless forms of the governing conservation equations for a buoyancy-driven, laminar natural convection under steady-state conditions are expressed in the forms:

Mass:

$$\frac{\partial U}{\partial X}+\frac{\partial V}{\partial Y}=0 \tag{1}$$

X-momentum:

$$U\frac{\partial U}{\partial X}+V\frac{\partial U}{\partial Y}=-\frac{\partial P}{\partial X}+\mathrm{Pr}\left(\frac{\partial^2 U}{\partial X^2}+\frac{\partial^2 U}{\partial Y^2}\right) \tag{2}$$

Y-momentum:

$$U\frac{\partial V}{\partial X}+V\frac{\partial V}{\partial Y}=-\frac{\partial P}{\partial Y}+\mathrm{Pr}\left(\frac{\partial^2 V}{\partial X^2}+\frac{\partial^2 V}{\partial Y^2}\right)+RaPr\theta) \tag{3}$$

Energy:

$$U\frac{\partial \theta}{\partial X}+V\frac{\partial \theta}{\partial Y}=\left(\frac{\partial^2 \theta}{\partial X^2}+\frac{\partial^2 \theta}{\partial Y^2}\right) \tag{4}$$

using the following non-dimensional variables:

$$X=\frac{x}{H},\ Y=\frac{y}{H},\ U=\frac{uH}{\alpha},\ V=\frac{vH}{\alpha},\ \theta=\frac{T-T_C}{T_H-T_C},\ P=\frac{pH^2}{\rho\alpha^2},\ Pr=\frac{v}{\alpha},\ Ra=\frac{g\beta(T_H-T_C)H^3}{\alpha v}$$

Boundary conditions:

On the base wall, U = V = 0; θ = 1

On the inclined walls, U = V = 0; θ = 0

The four pitch angles considered and their corresponding aspect ratio and Rayleigh number are as stated in Table 1.

Table 1. Parametric details of the enclosures.

Pitch Angle (ϕ)	14^o	20^o	25^o	35^o
Aspect Ratio, AR	0.25	0.36	0.47	0.7
Rayleigh Number (Ra)	$1.14\ x10^6$	$3.71\ x10^6$	$8.0\ x10^6$	$2.74\ x10^7$

The governing partial differential equations were discretized and a finite volume based CFD code, ANSYS FLUENT© (V18), was used to carry out the steady-state flow field and heat transfer predictions. Unstructured, very fine tetrahedron mesh, shown in Fig. 3 for the 25° pitch enclosure, was used with special attention given to the regions near the walls in order to properly resolve rapid changes within the resultant boundary layers. SIMPLE algorithm was employed for the pressure-velocity coupling. The QUICK scheme was adopted for spatial discretization of the momentum and energy equations. Convergence criteria were fixed at 10^{-5} for the continuity residual, and at 10^{-7} for the residuals of the momentum and energy equations.

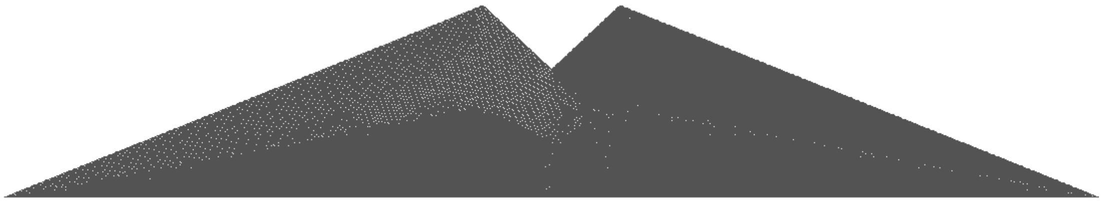

Fig. 3. Computational mesh for the 25° pitch enclosure .

Grid independence test was carried out to ensure the accuracy of the solution scheme and to determine an appropriate grid density. Many numerical runs were conducted for a given Rayleigh number at grids with different number of elements. A comparison of the maximum velocity magnitude to the number of elements was done as shown in Table 2. This implies a mesh with 76,000 elements was sufficient to produce grid independence in the 25° roof pitch enclosure.

Table 2. Grid independence test for the 25° roof pitch enclosure.

Number of elements	56,520	75,860	85,946
$\mathbf{U_{max}}$	0.20	0.21	0.21

3. RESULTS AND DISCUSSION

The plots of the predicted air velocity and temperature distribution within the attic are presented alongside the local and averaged Nusselt number variations among the results of the simulations. The velocity and temperature scales used are $U = \sqrt{g\beta(T_h - T_c)H}$ and $\theta = (T - T_c)/(T_h - T_c)$ respectively; making them range from zero to one.

3.1. Velocity Distribution

The predicted velocity distribution in the attic is shown in Figs. 4 and 5 for different pitch angles. Critical observation of the airflow patterns shows that the M shape and the aspect ratio, AR, which is proportional to the pitch angle, ϕ, of the enclosure have strong influence on the flow behaviour. At low pitch angle, rising hot air from the base wall hits the upper inclined cold walls quickly, splits in both directions and returns; thus forming counter-rotating cells. The number of the cells increases with decreasing pitch angle. The convection currents create a system that shows peak values of the flow velocity at the regions where the counterrotating cells rub each other. The strength of a rotating cell reduces from the outer circumference towards the centre.

The results show that, in comparison with normal pitch roofs, the 'M' shape of the roof affects the velocity distribution. In the 14°-pitch enclosure, Fig. 4(a), twenty vortices are symmetrically arranged on each half of the roof as divided naturally by the inverted vertex. The size and strength of the vortices reduce from the midsection towards the bottom corners. In Fig. 4(b), for the 20° roof pitch, the number of vortices has reduced to sixteen while still maintaining the symmetrical arrangement. The 30° roof pitch, Fig. 4(c), has twelve rotating cells that have become generally larger. Fig. 4(d), for the 35°, still shows symmetric flow structure with four large counterrotating cells in each half of the enclosure. Though, the two new upper vertices are expected to be quiescent, in each half, a small cell is found to have developed above the largest cell. This may be as a result of the splashing of the vortices on the sides of the middle vee. Results obtained in this study are analogous to those in Holtzman *et al* (2000) that reported flow visualization experimental results for a smoke-filled isosceles triangular enclosure heated from below that the flow pattern becomes multi-cellular and the number of counter-rotating cells increases with Rayleigh number.

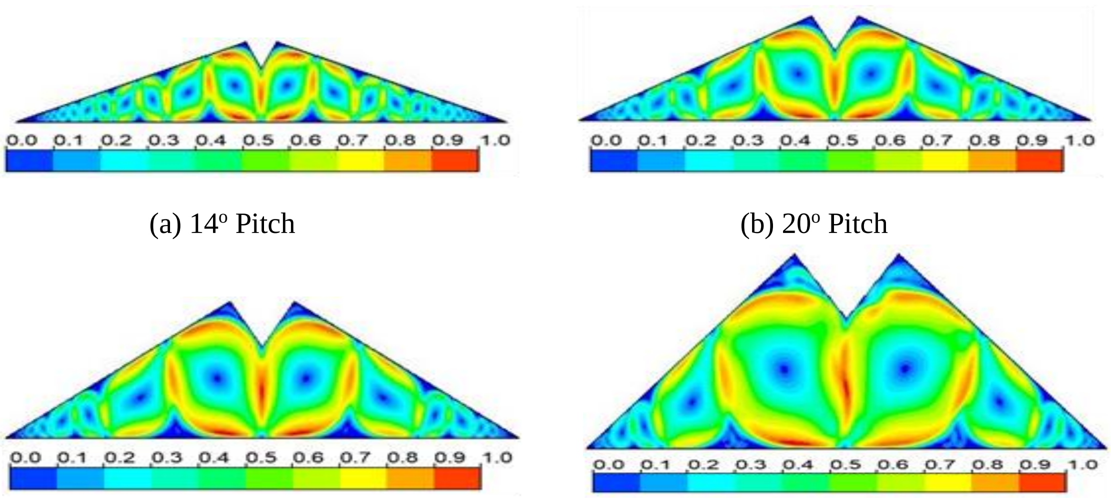

(a) 14° Pitch (b) 20° Pitch

(c) 25° Pitch (d) 35° Pitch

Fig. 4. Velocity contour plots.

In Fig. 5(a-d), plots of values of predicted velocity at the midheight (Y= 0.5H) of the attic for different pitch angles are presented. The velocity peaks where adjacent counterrotating cells rub each other and lowest at the core of the cells thereby forming a sequence that mimics the flowfield. The distance between two peaks, which forms a cycle, corresponds to a cell diameter. As the roof pitch increases, the size of the twin vortices at the central area increase by 4%. Fig. 5 thus enables the size of a cell and its intensity at a position in an attic of a particular pitch to be predicted. Such plot at a cross-section in an enclosure permits the prediction of the convection currents that could guide in the proper ventilation of the attic space and the best arrangement of food crops in the attic when used for drying.

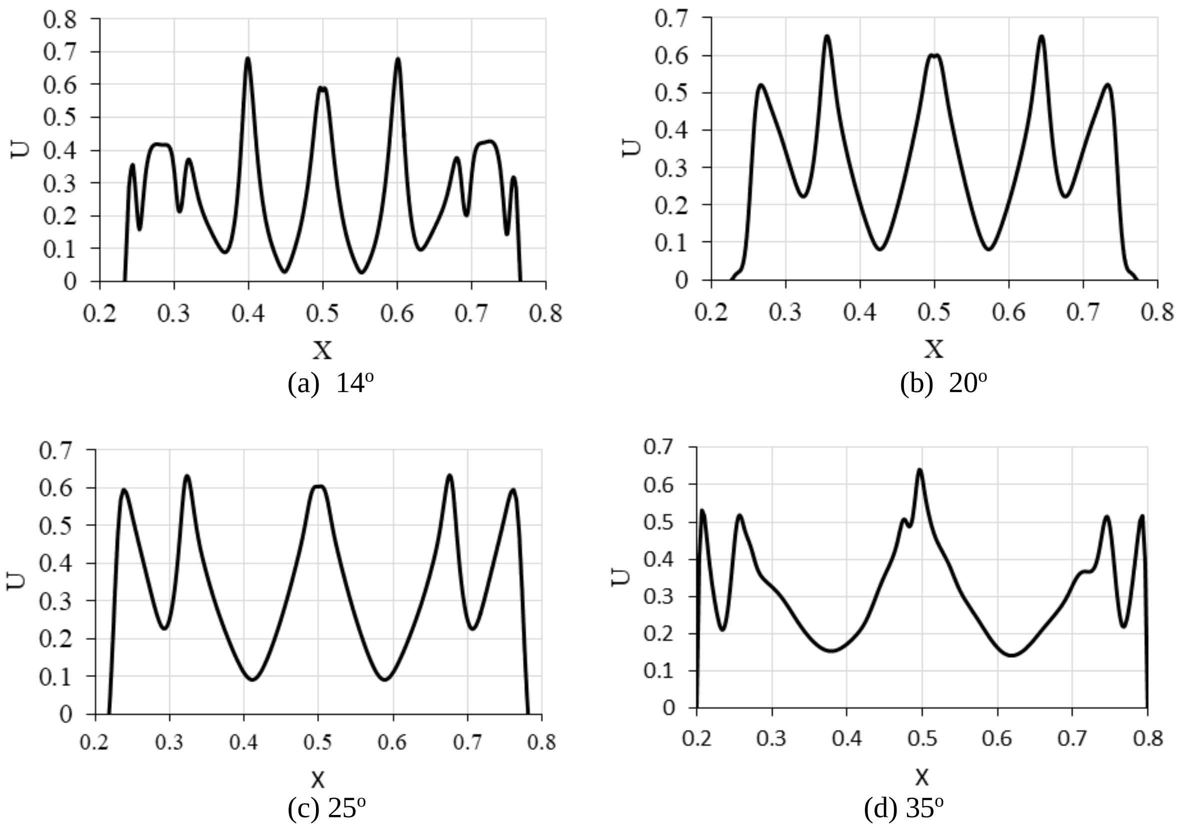

Fig. 5. Air velocity across midheight (Y= 0.5H) of different enclosures

Fig. 6 shows air velocity profile at the vertical centerline (X = 0.5L) of each enclosure presented together. In all the enclosures, the centerline coincides with a cold jet between the two central vortices. Velocity varies as heavy, cold air, under gravity, accelerates downward from the edge of the vee, reaches a peak at the midheight, and then gradually reduces to almost zero when it hits the basewall. Unlike the profiles in Fig. 5 that changes with the roof pitch, the vertical profile follows a similar parabolic shape irrespective of the roof pitch. This helps to predict the velocity value at any point along the cross-section and to know that maximum value is at the centre of each enclosure.

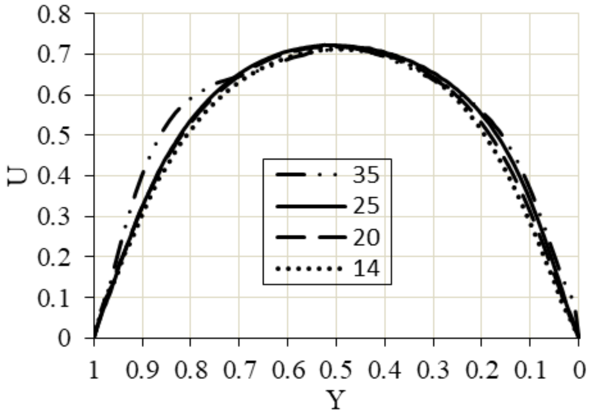

Fig. 6. Air velocity at midlength (X=0.5L) of different enclosures

3.2. Temperature Field

As shown in Figs. 7-9, the temperature distribution within the cavity shows a pattern of rising hot air from the heated base wall in form of thermal plumes, splashing onto the cold inclined walls above where a major part of the heat convected is lost, splitting in either directions and returning in form of cold jets to the base wall to form convection currents. The thermal plumes indicate regions where adjacent counterrotating cells rub each other. However, as part of the distinguishing features of the M-shaped roof, due to the middle vee, the two cells at the central portion rotate in such manner that they bring down a cold jet, unlike in a standard pitch roof where a thermal plume is formed. In all the enclosures, the number of thermal plumes is half the number of cells. As the roof pitch increases, the cell size increases, and the plume gets thicker while their number reduces.

In Fig. 7(a) for the 14^{o} roof pitch, the average temperature across the attic is high because the high number of rotating cells aid thorough circulation of hot air. The closeness of the cold wall to the hot ceiling enables the quenching effect of the cold wall to be limited to areas along the surface of the inclined wall leading to thin thermal boundary layer. As the roof pitch increases, the boundary layers along the walls thicken. In the 35^{o} pitch cavity, Fig. 7(d), the temperature field remains the same with the number of plumes now reduced to only four and lower average temperature. The temperature within the upper vertices approaches that of the cold wall as the effect of the heating from the base wall reduces with roof pitch increase.

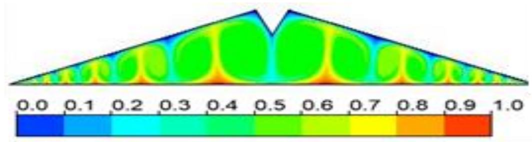

(a) 14°

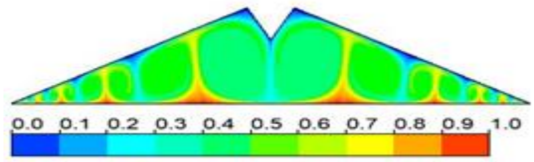

(b) 20°

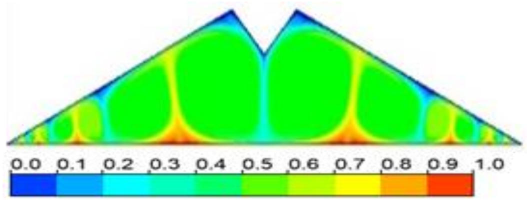

(c) 25°

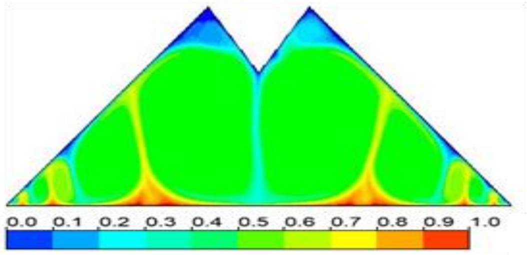

(d) 35°

Fig. 7. Temperature contour plots.

Temperature profile across the midheight (Y = 0.5H) of each enclosure is presented together in Fig. 8. The distance between a crest, which connotes a point on the plume and a trough, which is a point on the cold jet forms the diameter of a cell. Therefore, the size of a cell could easily be determined from the plot. The mean temperature at that cross-section is seen to be $\theta = 0.54$. Such profile at other cross-sections could be obtained to determine thermal condition at a region within similar enclosures. Fig. 8 also shows that the cold jet at the middle has the same dimensionless value in each enclosure and therefore, practical prediction of the thermal condition at the middle of the enclosures becomes possible.

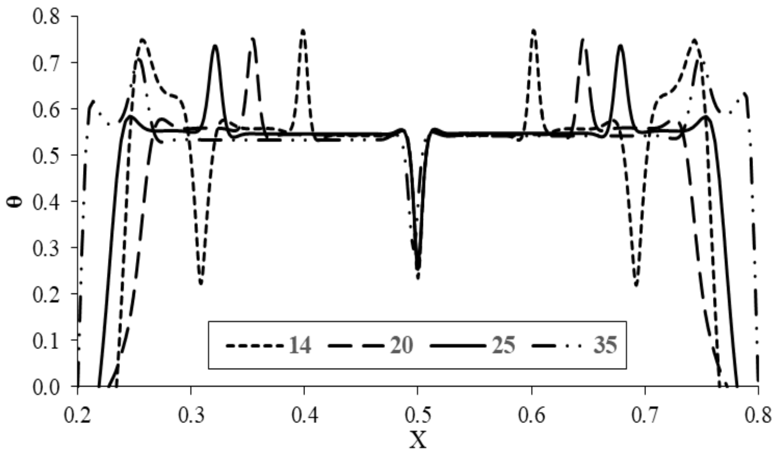

Fig. 8. Dimensionless temperature across midheight (Y= 0.5H) of different enclosures.

At the midlength (X = 0.5L), air temperature as the cold jet drops for the enclosure is presented in Fig. 9. From the end of the middle vee, the temperature increases gradually as the cold jet move towards the hot base wall and sharply increases within the thermal boundary layer of which its thickness is about 0.05 of the enclosure height. Similar to Fig. 6, the temperature profile follows a similar pattern irrespective of the roof pitch except for the 35° which deviated slightly due to low turbulence. This helps to predict the value of the temperature at any point along the cross-section.

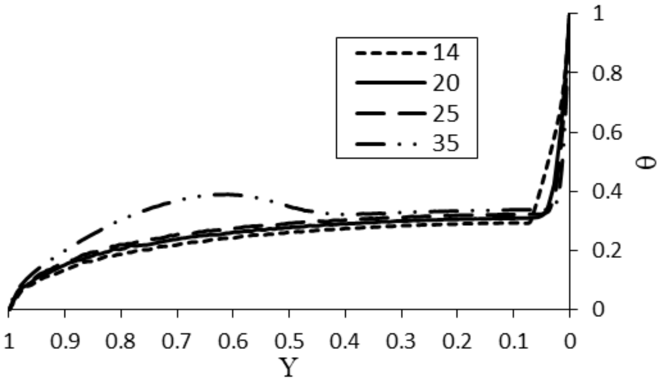

Fig. 9. Air temperature at midlength (X=0.5L) of different enclosures.

3.3. Heat Transfer

The local Nusselt number variation along the hot and cold walls which represents changes in the local heat transfer coefficient aids the understanding of the heat transfer within the enclosures. It can be defined as:

$$Nu_x = \frac{h_x L}{k} \tag{5}$$

and, the averaged Nusselt number along a wall as:

$$\overline{Nu} = \frac{\bar{h}L}{k} \tag{6}$$

where the length of the base wall L, which is common to the enclosures, is chosen as the characteristic length.

The variation of the values of the local Nusselt number along the hot basewall (Fig.10a) and cold roof (Fig.10b) of different pitch angles is presented. On both walls, the sequential sinusoidal patterns of the variation shows that the rate of heat transfer within the attic links directly with the attaching and detaching processes of the thermal plumes at the hot wall and the cold jets at the cold wall. Heat transfer rate goes to lowest value where two counter-rotating cells disconnected air at the same temperature as the walls thereby creating a region of near-zero temperature gradient at the point. The peak values correspond to points where cold jets splash on the hot horizontal base wall and thermal plumes splash on the cold roof. Near the lower corners, the values of *Nu* are relatively high due to the proximity of the cold and hot walls. Nevertheless, that does not affect the overall thermal efficiency of the system.

Looking closely at the plots, specifically at the midlength of the enclosure, the vee formed by the ‘M’ shape of the roof affects the heat distribution at the midsection. In Fig. 10(a), the middle cold jet moving downward from the vee under gravity, with relatively high speed splashes on the basewall with a force that create a little disturbance which becomes more pronounce as the pitch angle increases. On the other hand, in Fig. 10(b), the plots form an ‘m’ at the middle, X=0.5. This is because the cell on the right side of the vee rotating anticlockwise after splashing on the roof at X=0.6, exchanging heat, again splashes on the vee to repeat heat exchange with it before flowing downward as a cold jet, having lost most of its heat. The same heat exchange process is similarly done by the cell on the left side of the vee. These together formed the ‘m’ shape on the *Nu* plots.

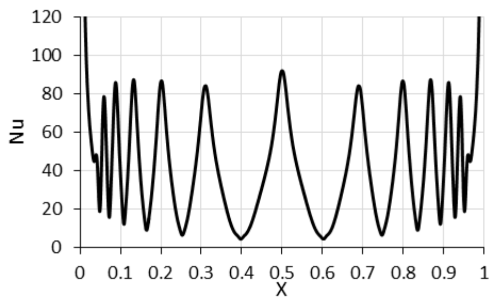

14^{o}

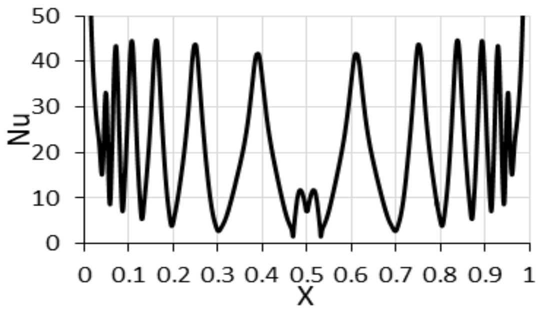

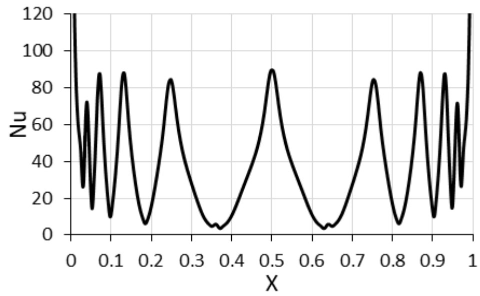

20^{o}

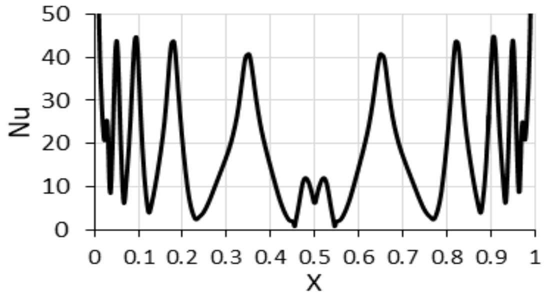

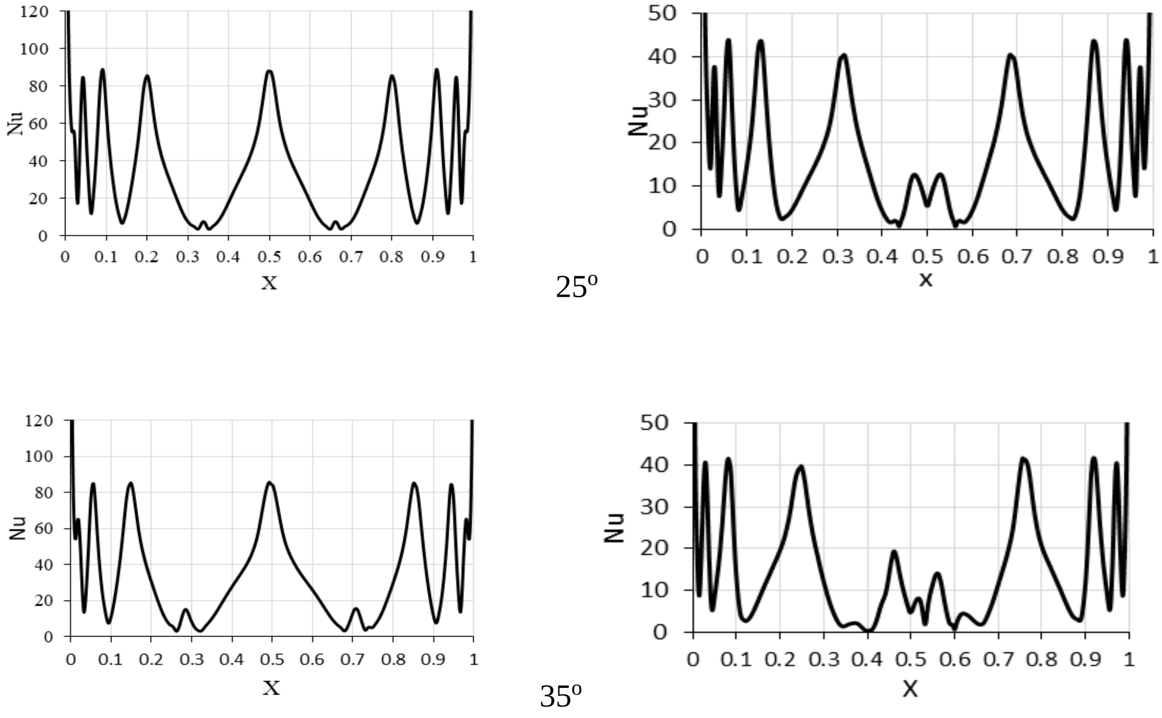

(a) Hot Basewall (b) Cold Roof

Fig. 10. Local Nusselt number plots along the (a) hot basewall, and (b) cold roof for different pitch angles.

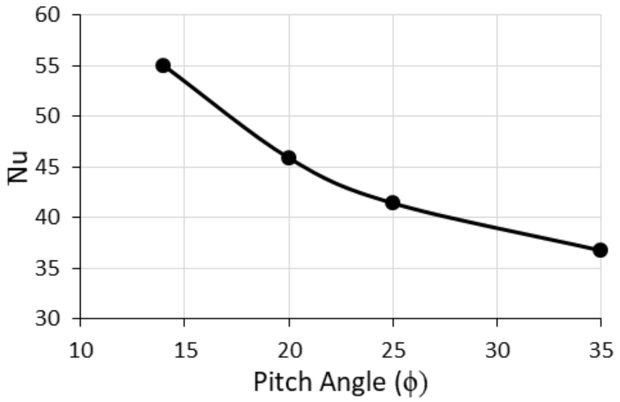

Fig. 11. Mean Nusselt number with pitch angles.

Fig. 11 shows the plot of mean *Nu* of the hot basewall against the roof pitch which correspond to the total heat transfer rate in the enclosures. The relation is quasi-linear. The thermal power driven by the vortices to the cold walls reduces significantly between 14° and 35° pitch angles. Specifically, the value of the mean *Nu* for the hot base wall in the 35° pitch is just about a third of that in the 14° pitch. The reason for this is apparent. As the pitch angle increases, the distance between the hot and cold walls increases. Also, the length of the inclined cold wall has increased by 20% and consequently the major part of the cavity becomes colder. As a result, the rate of heat transfer between the walls reduces. The practical significance of the results is that when the aim is to minimize heat loss from heated space below the ceiling into the attic, the roof pitch should be made high enough. But if the focus is drying of agricultural produce as in the rural communities in the developing world, the roof pitch should be made low.

4. CONCLUSION

Natural convective heat transfer in M-shaped pitched roofs has been investigated using CFD approach with the aim of determining the flow field and thermal characteristics of the attic when heated through the ceiling for certain pitch angle range while keeping the enclosure base-length unchanged. The M-shaped of the roof and its pitch angle have strong influence on the results obtained. In all the enclosures, symmetrically-arranged multiple counterrotating cells and thermal plumes occurs. The number of the cells however decreases with increasing pitch angle. The size and strength of the rotating cells also reduce from the midsection towards the bottom corners. Unlike in a normal pitch roof where the cells at the central portion forms a thermal plume, the middle vee makes the two central cells to bring down a cold jet. As the roof pitch increases, the cell size increases, and the plume gets thicker while their number reduces. Heat transfer rate is enhanced with decreasing value of the roof pitch.

The practical significance of the results is that when the aim is to minimize heat loss from heated space below the ceiling into the attic, the roof pitch should be made high enough. But if the focus is drying of agricultural produce as in the rural communities in the developing world, the roof pitch should be made low. This work will therefore be useful to rural farmers in developing countries and building designers in their choice and installation of insulation materials for controlling heat losses.

5. REFERENCES

Akinsete, V.A. and Coleman, T.A., (1982) ‘Heat transfer by steady laminar free convection in triangular enclosures’, International Journal of Heat Mass Transfer, 25, 991.

Amrani, A., Dihmani, N., Amraqui, S., and Mezrhab, A., (2017) ‘Analysis of combined natural convection and thermal radiation heat transfer in a triangular shaped roof for hot climates’, Journal of Materials and Environmental Sciences, 8(8), 3013-3027.

Anderson, T.N., Duke, M., and Carson, J.K., (2010) ‘Experimental determination of natural convection heat transfer coefficients in an attic shaped enclosure’, International Communications in Heat and Mass Transfer, 37(4), 360-363.

Asan, H., and Namli, L., (2000) 'Laminar Natural Convection in a Pitched Roof of Triangular Cross-Section: Summer Day Boundary Conditions', Journal of Energy and Building, 33, 69-73.

Ching, Y.C., Oztop, H.F., Rahman, M.M., Islam, M.R., and Ahsan, A., (2012) 'Finite element simulation of mixed convection heat and mass transfer in a right triangular enclosure', International Communications in Heat and Mass Transfer, 39(5), 689-696.

Cui, H., Xu, F., Sahad, S., and Liu, Q. (2019) 'Transient free convection heat transfer in a section triangular prismatic enclosure with different aspect ratios', International Journal of Thermal Sciences, 139, 282-291.

Das, D., Roy, M., and Basak, T., (2017) 'Studies on natural convection within enclosures of various (non- square) shapes- A review', International Journal of Heat and Mass Transfer, 126, 356-406.

Das, S., and Morsi, Y., (2002) 'Natural Convection Inside Dome Shaped Enclosures', International Journal of Numerical Methods for Heat and Fluid Flow, 12(2), 126-141.

Flack, R. D., (1980) 'The experimental measurement of natural convection heat transfer in triangular enclosures heated or cooled from below', Journal of Heat Transfer, 102, 770-772.

Gray, D.D., and Giorgini, A., (1976) 'The validity of the Boussinesq approximation for liquids and gases', International Journal of Heat and Mass Transfer, 19, 545-551.

Holtzman, G.A., Hill, R.W., and Ball, K.S. (2000) 'Laminar natural convection in isosceles triangular enclosures heated from below and symmetrically cooled from above', Journal of Heat Transfer, 122(3), 485-491.

Kamiyo, O. M., Angeli, D., Barozzi, G.S., Collins, M.W., Olunloyo, V.O.S. and Talabi, S.O., (2010) 'A comprehensive review of natural convection in triangular enclosures', Applied Mechanics Review: Transactions of ASME, 63(060801), 13pages.

Kamiyo, O.M., Angeli, D., Barozzi, G.S., and Collins, M.W., (2014) 'Natural convection in asymmetric triangular enclosures heated from below', Journal of Physics: Conference Series, 547, 1-10.

Mahmoodi, M., (2011) 'Natural convection heat transfer in right triangular enclosures with a cold inclined wall and a hot vertical wall', Heat Transfer Research, 42(3), 217-231.

Mahmoudi, A., Mejri, I., Abbassi, M.A., and Omri, A., (2013) 'Numerical study of natural convection in an inclined triangular cavity for different thermal boundary conditions: application of the lattice Boltzmann method, Fluid Dynamic Material Process', 9, 353-388.

Mehryan, S.M., Mohammad, G., Reza, K.F., Ahmad, H., and Mohsen, I., (2020) 'Free convection in a trapezoidal enclosure divided by a flexible partition', International Journal of Heat and Mass Transfer, 149, 119186, 14 pages.

Michels, C., Güths, S., Deivis, L.M., and Lamberts, R., (2018) 'Development of an experimental test rig for the evaluation of the thermal performance of building roofs', Energy and Buildings, 180, 32–41.

Mirabedin, S., (2016) 'CFD modelling of natural convection in right–angled triangular enclosures', International Journal of Heat Technology, 34(3), 503-506.

Oztop, H.F., Varol, Y., Koca, A., and Firat, M., (2012) 'Experimental and numerical analysis of buoyancy-induced flow in inclined triangular enclosures', International Communications in Heat and Mass Transfer, 39, 1237–1244.

Penot, F., and N'Dame, A. (1992) 'Successive bifurcations of natural convection in a vertical enclosure heated from the side', Heat Transfer: Proceedings of the 3rd UK National Conference and First European Conference on Thermal Sciences, Birmingham, UK, 1, 507-513.

Raj, R., Pradyumna, K. C., Rakshith, B.R., Nithin, R.B., and Karthik, S.R. (2018) 'Combined natural convection and surface radiation inside vented triangular enclosure- an experimental study'. International Conference on Research in Mechanical Engineering Sciences. 144, 04019, 8 pages.

Ridouane, E. H., Campo, A., and McGarry, M. (2005) 'Numerical computation of buoyant airflows confined to attic spaces under opposing hot and cold wall conditions', International Journal of Thermal Sciences, 44, 944–952.

Saha, S.C. and Khan, M.M.K., (2011) 'A review of natural convection and heat transfer in attic-shaped space', Energy and Building, 43, 2564-2571.

Saha, S.C., and Gu, Y.T. (2015) 'Natural convection in a triangular enclosure heated from below and non-uniformly cooled from top', International Journal of Heat and Mass Transfer, 80, 529–538.

Saha, S.C., Patterson, J.C., and Lei, C.W., (2010a) 'Natural convection and heat transfer in attics subject to periodic thermal forcing, International Journal of Thermal Sciences, 49(10), 1899-1910.

Saha, S.C., Patterson, J.C., and Lei, C.W., (2010b) 'Natural convection in attics subject to instantaneous and ramp cooling boundary conditions', Energy and Buildings, 42(8), 1192-1204.

Sieres, J., Campo A., and Martinez-Suarez, J.A., (2016) 'Natural convection air flow in vertical upright –angled triangular cavities under realistic thermal boundary conditions', Journal of Thermal Science, 20(5), 1407-1420.

Triveni M.K., Sen D., and Panua R.S. (2014) 'Laminar natural convection for thermally active partial side walls in a right-angled triangular cavity', Arabian Journal of Science and Engineering, 39, 9025-9038.

Triveni, M.K., Sen D., and Panua R.S. (2015) 'Natural convection in a partially heated triangular cavity with different configurations of cold walls, Arabian Journal of Science and Engineering, 40, 3285-3297.

Wang, S., and Shen, Z. (2012) 'Effects of roof pitch on air flow and heating load of sealed and vented attics for gable-roof residential buildings', Sustainability, 4(9), 1999-2021.

Wang, S., Shen, Z., and Gu, L. (2012) 'The impact of roof pitch and ceiling insulation on cooling load of naturally-ventilated attics', Energies, 5(**7**), 2178-2196.

Yesiloz, G. and Aydin, O., (2013) 'Laminar natural convection in right-angled triangular enclosures heated and cooled on adjacent walls', International Journal of Heat and Mass Transfer, 60, 365-374.